# Estimation of SW Flux Absorbed at the Surface from TOA Reflected Flux

ZHANQING LI* AND H. G. LEIGHTON

*Department of Atmospheric and Oceanic Sciences, McGill University, Montreal, Quebec, Canada*

KAZUHIKO MASUDA AND TSUTOMU TAKASHIMA

*Meteorological Research Institute, Tsukuba, Ibaraki, Japan*

(Manuscript received 21 July 1991, in final form 17 March 1992)

ABSTRACT

Measurements of radiation budgets, both at the top of the atmosphere (TOA) and at the surface, are essential to understanding the earth's climate. The TOA budgets can, in principle, be measured directly from satellites, while on a global scale surface budgets need to be deduced from TOA measurements. Most methods of inferring surface solar-radiation budgets from satellite measurements are applicable to particular scene types or geographic locations, and none is valid over highly reflective surfaces such as ice or snow. In addition, the majority of models require inputs such as cloud-optical thickness that are usually not known.

Extensive radiative transfer modeling for different surface, atmospheric, and cloud conditions suggests a linear relationship between the TOA-reflected flux and the flux absorbed at the surface for a fixed solar zenith angle (SZA). The linear relationship is independent of cloud-optical thickness and surface albedo. Sensitivity tests show that the relationship depends strongly on SZA and moderately on precipitable water and cloud type. The linear relationship provides a simple parameterization to estimate surface-absorbed flux from satellite-measured reflected flux at the TOA. Unlike other models, the present model makes explicit use of the SZA. Precipitable water is included as a secondary parameter. Surface-absorbed fluxes deduced from this simple parameterized model generally agree to within 10 W $m^{-2}$ with the absorbed fluxes determined from detailed radiative transfer calculations, without including information on the presence or absence of cloud, cloud type, optical thickness, or surface type.

## 1. Introduction

The importance of accurate knowledge of the surface radiation budget (SRB) is well known and has been discussed widely (e.g., Suttles and Ohring 1986). Although there is a long history of ground-based radiation measurements, the spatial coverage is, at best, sparse and for large regions entirely absent. There are, for example, few measurements over the two-thirds of the earth's surface that is covered by oceans, as well as over the polar regions, which may be particularly sensitive to climate change due to greenhouse warming. Satellite data have the advantage of being globally homogeneous and having high spatial and temporal resolution. To exploit the potential of satellite measurements the World Climate Research Programme (WCRP) established a SRB project whose objective is to derive the global SRB climatology from satellite measurements with an accuracy of 10 W $m^{-2}$ for fluxes averaged over a month and regions of 250 × 250 $km^2$ (Suttles and Ohring 1986). While meeting this goal for longwave radiation is a formidable task, considerable progress has been made toward meeting the objective for shortwave radiation.

Techniques to derive insolation at the surface have been reviewed by Schmetz (1989). The methods can be separated into two classes: empirical methods such as those used by Fritz et al. (1964), Tarpley (1979), and Klink and Dollhopf (1986); and physical methods, such as those described by Gautier et al. (1980), Moser and Raschke (1983), Pinker and Ewing (1985), Buriez et al. 1986, and Dedieu et al. (1987). The empirical methods develop regressions based on simultaneous and collocated satellite-radiance and surface-irradiance data, while the physical models interpret satellite-measured radiances in terms of scattering, reflection, and absorption parameters that are subsequently used in radiative transfer models or parameterized models to determine atmospheric transmittance and, hence, insolation.

However, for many purposes, including climate studies, it is net surface radiation rather than insolation that is significant. Net radiation is usually determined by combining the measurement of insolation with an

* Present affiliation: Canada Centre for Remote Sensing, 561 Booth Street, Ottawa, KIA OY7 Canada.

*Corresponding author address:* Dr. H. G. Leighton, Department of Atmospheric & Oceanic Sciences, McGill University, 805 Sherbrooke Street West, Montreal, H3A 2K6 Quebec, Canada.

© 1993 American Meteorological Society

independent estimate of surface albedo. As pointed out by Cess and Vulis (1989), the uncertainties associated with each of these quantities may lead to large errors in the value of the net surface solar radiation. An alternative approach is to attempt to deduce the net solar flux at the surface directly from the net solar flux at the TOA without explicit knowledge of the surface albedo. Based on climate model results, Ramanathan (1986) found a simple proportionality between the net fluxes at the TOA and surface. Cess and Vulis (1989), using more accurate delta-Eddington model radiative-transfer calculations, found that the relationship was linear but required an offset. The relationship was subsequently verified by collocated surface measurements made by radiometers mounted on a tower and TOA measurements made by the ERBE radiometer under clear skies (Cess et al. 1991). Their theoretical study shows that the relationship is moderately sensitive to atmospheric water vapor and aerosol content but very sensitive to the nature of the surface and cloud-optical thickness. Since cloud-optical thickness and surface type cannot be determined with high accuracy by satellite measurement, the application of the linear relationship to the estimation of surface net solar flux has been restricted to clear-sky conditions over known surface types (Cess et al. 1991). The key factor, which gives rise to the strong sensitivity, is the SZA, which is treated as an implicit variable in the relationship. The present work gives an alternative linear relationship between the TOA-reflected flux and surface-absorbed flux, which is based on comprehensive radiative-transfer calculations. The difference between this approach and the approach of Cess and Vulis (1989) is that here the SZA is included explicitly. This results in the important improvement that the relationship is independent of cloud-optical thickness and surface albedo and so can be used to infer the net solar flux at the surface under overcast skies.

The model and input data that are used to conduct radiative-transfer simulations are described in section 2. Section 3 discusses the modeling results and establishes the new linear relationship. A physical rationale for the new linear relationship is also given in this section. The sensitivity of the relationship to precipitable water, cloud type, surface type, and aerosol is examined in section 4. A parameterized model is described in section 5, and an error analysis is given in section 6. The conclusions are contained in section 7.

## 2. Model and input data

Radiative transfer simulations are conducted with a doubling–adding model applied to a plane-parallel vertically inhomogeneous atmosphere–surface system (Masuda and Takashima 1988, 1990). The code has been tested by comparing results with the results from another code for cloud-free conditions (Masuda and Takashima 1988). Also, energy-conservation tests for calculations of the transfer through a nonabsorbing cloud have given negligible errors.

Optical thicknesses due to molecular absorption are obtained from transmittances computed by LOWTRAN 6 (Kneizys et al. 1983). The scattering phase function is an optical thickness-weighted mean of the phase functions for molecular scattering, aerosol scattering, and scattering by cloud droplets. Absorption is expressed in terms of a single scattering albedo determined from the ratio of the optical thickness due to scattering by molecules, aerosol and cloud droplets, to the total optical thickness. The optical properties of water cloud droplets are taken from a tabulation given by Stephens (1979), the optical properties of the aerosol are calculated from Mie theory, and the optical properties of ice crystals are computed by applying the geometric optics approximation. Details of the calculations for horizontally oriented ice crystals are given in Masuda and Takashima (1990). The extraterrestrial solar-spectrum data, compiled by Iqbal (1983), are adopted. For the radiative-transfer calculations, the solar spectrum from 0.285 to 5.0 $\mu$m is divided into 108 wavelengths consisting of 83 unequal intervals from 0.285 to 2.5 $\mu$m and 25 equal intervals of 0.1 $\mu$m beyond 2.5 $\mu$m.

The original objective of this study was to develop a model to estimate surface net flux specifically for the polar regions, and so a subarctic summer-model atmosphere (McClatchey et al. 1971) is employed. The aerosol model 3 of Blanchet and List (1983) for Arctic Haze is also included in some of the simulations. It was subsequently found that the method could be applied more generally. Results are, therefore, also given for additional water vapor loadings obtained by scaling the subarctic model water vapor profile and for the complete range of SZAs, except for snow- and ice-covered surfaces in which case results are given only for SZAs greater than 45°.

Four surface types are selected: ocean, land, desert, and ice/snow. The spectral albedo of the ocean is calculated by the method of Masuda and Takashima (1988). The ice/snow spectral albedo is computed using the doubling–adding code for ice crystal properties obtained by following the approach of Wiscombe and Warren (1980). Mean grain sizes of 50, 200, 1000, and 2000 $\mu$m and a snow/ice depth of 2 m are assumed to simulate fresh, old, nearly melting, and melting snow or ice, respectively. To allow for anthropogenic contamination, trace amounts of graphitic soot with a mass fraction of 0.05 ppmw are included (Warren and Wiscombe 1980; Tsay et al. 1989). For the present calculations, the large variety of different land surfaces are spanned by choosing surfaces of desert and bog, the latter taken to represent vegetated land. In terms of their optical properties, these are the two most extreme categories of land that were considered by Cess and Vulis (1989). Figure 1 illustrates the spectral dependence of the surface albedo at an SZA of 60° for

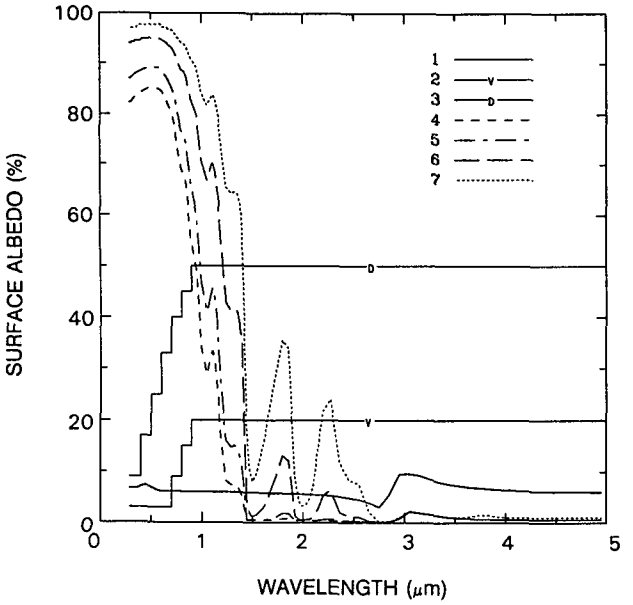


FIG. 1. Spectral variations of surface albedo at an SZA of 60° for (1) ocean, (2) vegetated land, (3) desert, and snow with varying mean grain sizes: (4) 2000 μm, (5) 1000 μm, (6) 200 μm, and (7) 50 μm, which approximately represent melting, near melting, aging, and new snow, respectively.

the various surface types. The corresponding broadband surface albedos are 6.6%, 9.8%, 35%, 63%, 69%, 79%, and 86% for ocean, vegetated land, desert, and snow/ice of grain sizes decreasing from 2000 μm to 50 μm. Except for vegetated land and desert, which are assumed to scatter isotropically, surface reflectivity is a function of SZA.

Four types of clouds are included in the simulations: three water clouds and one cirrus cloud. The water cloud optical properties are those for the St-II, Sc-II, and Cu models compiled by Stephens (1978), as given in Stephens (1979), and the cirrus cloud-optical properties are those of the CL 2 cloud defined by Masuda and Takashima (1990). These particular cloud types were selected not only because they are morphologically distinct but their optical properties are equally diverse. The St-II and Cu models represent the two extreme models in terms of single-scattering albedo and the asymmetry factor of the eight models given by Stephens. The cirrus cloud model is for a cloud composed of columnar hexagonal ice crystals, randomly oriented with their long axes in the horizontal plane. Optical thicknesses at a wavelength of 0.55 μm are taken to be 5, 10, 20, and 40 for water clouds and 1.25, 2.5, 5, and 10 for the cirrus cloud.

The clear atmosphere is divided into six homogeneous layers (0–2.72, 2.72–5, 5–10, 10–20, 20–30, and 30–100 km), but for cloudy skies, nine layers are allowed. Altitudes of the boundaries of the top three layers for cloudy-sky simulations are the same as those for clear skies, while the remaining six lower layers are 0.0–0.8, 0.8–$C_{top}$, $C_{top}$–2.72, 2.72–5.44, 5.44–9.0, and 9.0–10 km. Water clouds are assumed to be present in layer 2, with cloud-top altitude $C_{top}$ given in Table 1, determined by the cloud-optical thickness and the volume-extinction coefficient. The St II cloud type with an optical thickness of 40 has $C_{top}$ larger than 2.72, and so in this case, the cloud is assumed to occupy the two layers 0.8–2.72 km and 2.72–$C_{top}$ km, with the fourth layer extending from $C_{top}$ to 5 km. Cirrus cloud is assumed to be in layer 6. Nearly 100 simulations are conducted by combining different atmospheric, cloud, and surface conditions. The results consist of the upward and downward fluxes at both the TOA and surface for up to 15 SZAs.

## 3. Relationships between TOA and surface fluxes

### *a. Cess and Vulis relationship*

Cess and Vulis (1989) showed that the net solar fluxes at the surface and TOA vary approximately linearly as the SZA changes. For a particular surface type they found that variations in the water vapor content of a factor of 2 and the presence or absence of a standard aerosol profile could be accounted for by a single linear fit to within about ±5%. If, in addition to allowing the water vapor and aerosol loading to change, the surface type is not specified but is allowed to be ocean, vegetated land, or desert, then the accuracy of a single linear fit is only about ±10%. These results formed the basis of parameterized relationships between the surface and TOA fluxes for clear skies and surfaces of vegetated land and ocean (Cess et al. 1991). Surfaces of snow and ice were explicitly excluded because of the variability in the albedo of snow/ice. The difficulty associated with the uncertainty in the relationship for snow/ice surfaces is illustrated in Fig. 2, which shows results of model calculations of the TOA net flux–surface net flux relationship for ocean and four different ice/snow surfaces. Clearly, without additional information no single expression can provide a useful method of deducing the flux absorbed at the surface from a TOA measurement. A similar situation exists for clouds. Figures 3 and 4 show the influence on the relationship of stratocumulus cloud of optical thickness, varying from 0 (clear skies) to 40, over ocean and fresh snow, respectively. The uncertainty in the flux absorbed at the surface for a particular value of the total flux ab-

TABLE 1. Altitudes (km) of the top boundary of cloud layer for three water cloud types with four optical thickness.

| | Optical thickness | | | |
|---|---|---|---|---|
| Cloud | 5 | 10 | 20 | 40 |
| St II | 1.13 | 1.46 | 2.11 | 3.43 |
| Sc II | 0.87 | 0.94 | 1.07 | 1.34 |
| Cu | 0.84 | 0.88 | 0.96 | 1.11 |

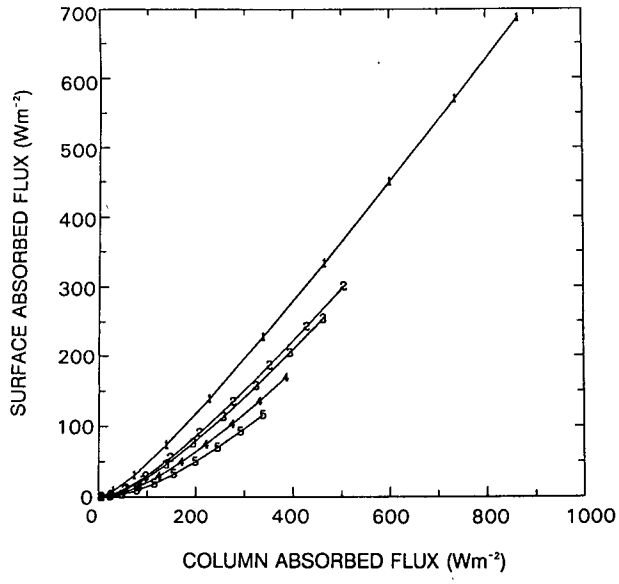


FIG. 2. Relationship between the flux absorbed at the surface and the flux absorbed by the column for (1) clear ocean, (2) melting snow, (3) near-melting snow, (4) aging snow, and (5) fresh snow, with precipitable water 2.1 cm and haze-optical thickness 0.05. The SZAs for the points represented by numbers along curves range from 90° to 45° from left to right.

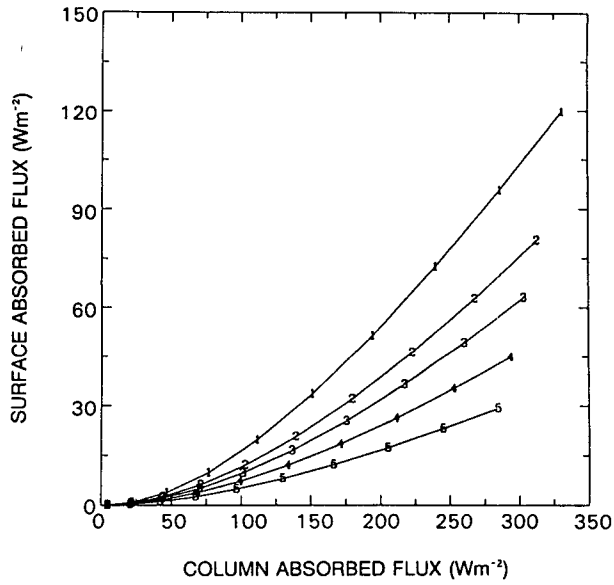


FIG. 4. Same as Fig. 3 but for Sc II over fresh snow and SZA ranging from 90° to 45°.

sorbed in the column can be as large as 200 W $m^{-2}$ over ocean and 60 W $m^{-2}$ over snow. Since there are major limitations on the reliability of satellite measurements of cloud-optical thickness and surface type, especially the nature of snow/ice surfaces, the usefulness of the method of parameterization of Cess et al. (1991) to obtain surface absorbed fluxes is limited.

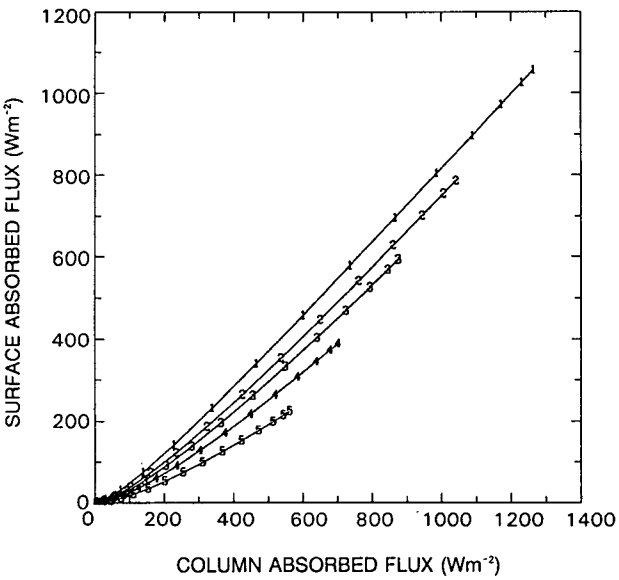


FIG. 3. Same as Fig. 2 but for Sc-II cloud of optical thickness 0, 5, 10, 20, and 40 given by curves 1, 2, 3, 4, and 5, respectively, over ocean. From left to right, the SZA changes from about 90° to 6°. Precipitable water content is equal to 1.6 cm, and haze-optical thickness is 0.05.

### b. *A new linear relationship*

The form of the relationship between the net solar fluxes at the TOA and the surface, used by Cess and Vulis (1989) and Cess et al. (1991), contains the SZA as an implicit variable. However, it is the SZA that has the dominant influence on the flux absorbed in the atmosphere and, thereby, on the relationship between the net fluxes at the TOA and surface. Moreover, of all the parameters, it is the SZA that is known most precisely. This suggests that a relationship that involves the SZA as an explicit parameter may be more successful.

Figure 5 shows the relationship between the outgoing flux at the TOA and the flux absorbed at the surface for the same conditions as Fig. 2 but with the SZA as an explicit parameter. For a particular SZA, the relationship between the fluxes is linear as the surface type changes from ocean to ice of different crystal sizes. The slopes of the lines are weakly dependent on the SZA. A similar result is found for cloudy skies, as is shown in Fig. 6 for the same conditions as Fig. 3. Again, for fixed SZAs the points corresponding to cloud-optical thickness varying from 0 to 40 lie along approximately parallel, straight lines.

If the irradiances in Figs. 5 and 6 are normalized by the incident irradiance at the TOA, then the lines in the figures can be expressed in the form

$$a_s = \alpha(\mu) - \beta(\mu)r, \qquad (1)$$

where $a_s$ is the fraction of the incident irradiance absorbed at the surface, $r$ the local planetary albedo, and $\mu$ the cosine of the SZA. The linear relationship given by (1) is consistent with the results of Schmetz (1984, 1989), who found that atmospheric absorption changes linearly with local planetary albedo for varying cloud-optical thickness; that is,

$$a_a = c_0(\mu) + c_1(\mu)r, \tag{2}$$

where $a_a$ denotes the fraction of the incident irradiance absorbed in the atmosphere. From the results of Monte Carlo calculations, Schmetz (1984) also found that the linear relationship is not altered by the presence of broken clouds, a result that was subsequently confirmed by the observations of Rawlins (1989).

The intercept and slope of (1) are related to the coefficients of Eq. (2) by

$$\alpha(\mu) = 1 - c_0(\mu) \tag{3}$$

$$\beta(\mu) = 1 + c_1(\mu). \tag{4}$$

For clear skies, $c_0$ and $c_1$ are measures of the absorption of the downward and upward fluxes, respectively. Because of scattering and absorption by cloud droplets, such a simple physical interpretation of $c_0$ and $c_1$ is not applicable to cloudy skies. Nevertheless, it will be useful, even for cloudy skies, to think of $c_0$ as being primarily a measure of absorption of downward flux above the cloud and as such to be dependent primarily on absorber concentrations above the cloud. To gain insight into the effect of the SZA on $c_0$ and $c_1$, the results in Figs. 5 and 6 are replotted in terms of $a_a$ and $r$ in Figs. 7 and 8, respectively. Consistent with the interpretation of $c_0$ given above, the intercept increases with SZA for both the clear-sky (Fig. 7) and cloudy-sky (Fig. 8) cases. For a nonabsorbing atmosphere, $c_0$ would be equal to zero. The slope of the lines in Figs. 7 and 8, $c_1$, is a measure of the coupling between absorption and reflection. For clear skies, $c_1$ is only weakly dependent on the SZA, but for cloudy skies, $c_1$ decreases significantly with increasing SZA. This is due

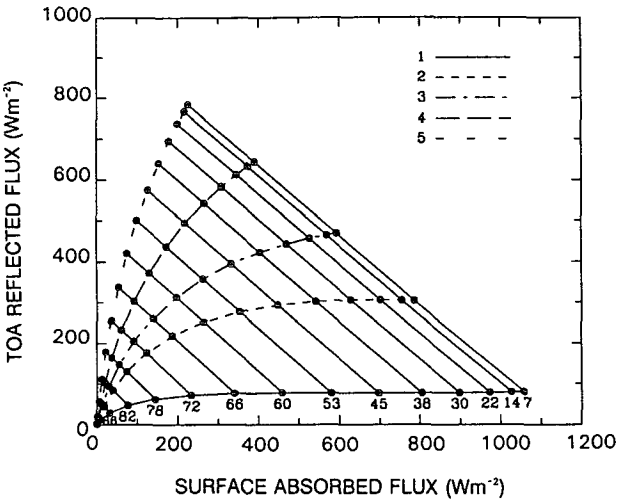


FIG. 6. Same as Fig. 5 but for the simulations of Fig. 3. Curves 1, 2, 3, 4, and 5 correspond to cloud-optical thicknesses of 0, 5, 10, 20, and 40, respectively.

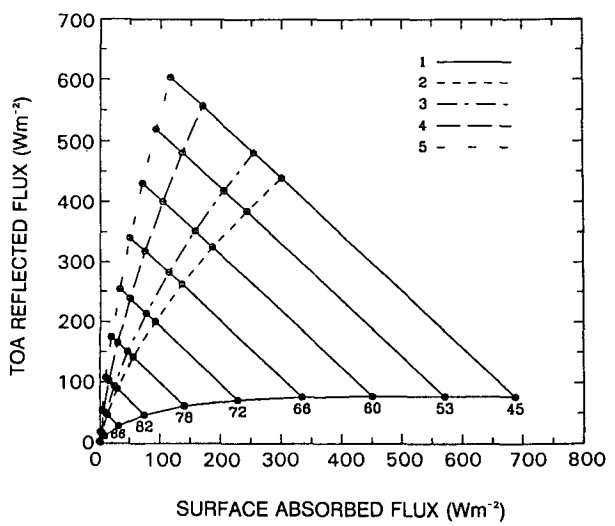


FIG. 5. Relationship between the flux absorbed at the surface and the flux reflected at the TOA for the simulations of Fig. 2. The curves 1–5 join points representing the results of calculations for surfaces of ocean, melting snow, near melting snow, aging snow, and fresh snow, respectively. The straight lines join points that are for the same SZA.

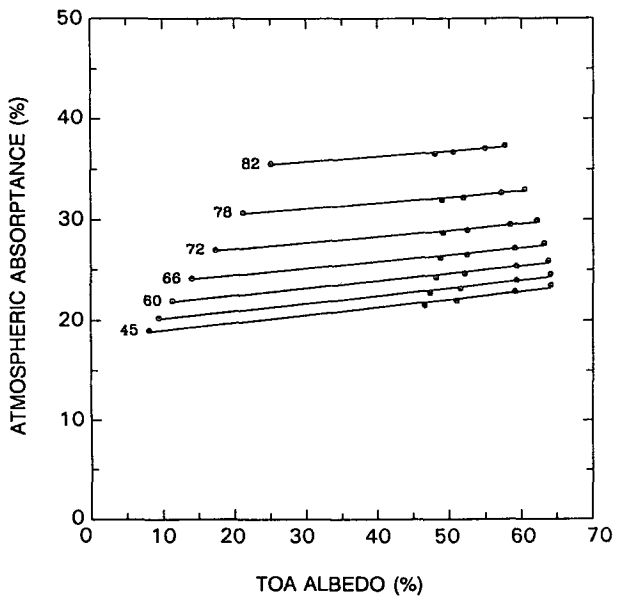


FIG. 7. Relationship between atmospheric absorptance and TOA albedo for the simulations of Fig. 2. The straight lines are fits to results for fixed SZAs but have different surfaces, specifically ocean, melting, near-melting, aging and fresh snow indicated by points from left to right along the lines.

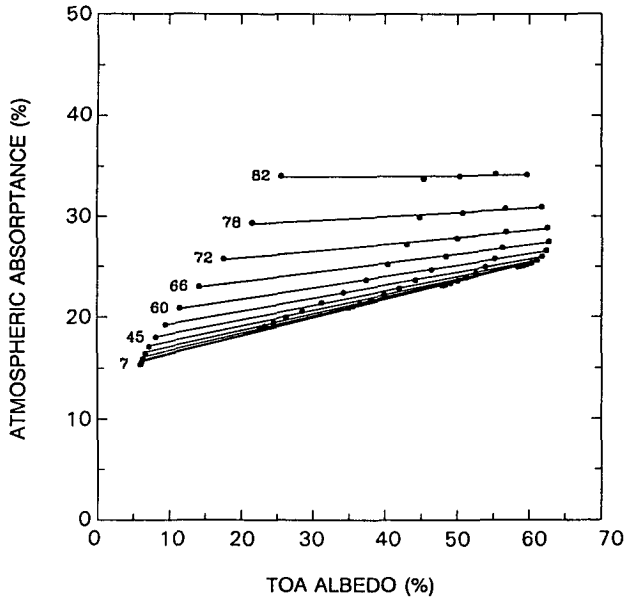


FIG. 8. Same as Fig. 7 but for the simulations of Fig. 3. Points from left to right along the regressional lines have cloud-optical thickness 0, 5, 10, 20, and 40.

to the difference in the effects of increase in cloud-optical thickness on atmospheric absorption and local planetary albedo. At large SZAs, the absorption saturates, so increases in optical thickness produce only small increases in absorption (Davies et al. 1984). In contrast, cloud reflection increases steadily with increasing cloud-optical thickness (Davies 1980) and, hence, the slopes of the lines in Fig. 8 decrease with increasing solar zenith angle.

The implication of these results is clear. To the extent that the linear relationships are independent of other atmospheric parameters, they will provide a useful method of determining absorption at the surface that is independent of the specific nature of the surface or cloud thickness. It remains to examine the sensitivity of the relationship to other parameters.

## 4. Sensitivity studies

### *a. Precipitable water*

Apart from clouds, the quantity that has the largest influence on the solar flux incident at the surface is the water vapor content of the atmosphere. Since the amount of water vapor directly influences the flux absorbed in the atmosphere, the water vapor content can be expected to have an influence on the relationship between the TOA flux and the net surface flux. To determine the effect of water vapor on this relationship, calculations are carried out for precipitable water amounts of 1.1, 1.6, 2.1, 3.1, and 5.1 cm, representing atmospheres ranging from a relatively dry polar-summer atmosphere to a moist tropical atmosphere. Lines through the points representing the results of these calculations for solar zenith angles varying from 7° to 78° for an ocean surface, and ice surfaces with different grain sizes, are shown in Fig. 9. Some combinations of surface, zenith angle, and precipitable water are recognized as being unrealistic. Again, the results can be represented by sets of almost parallel lines with the water vapor content having a significant influence on the intercept but only a slight effect on the slope. This result is expected from (1)–(4) since the intercept depends on $c_0$, which is a measure of the absorption of direct solar radiation by water vapor; whereas the slope is $-(1 + c_1)$, with $c_1$ a measure of the absorption of the upward solar radiation being small compared to 1. Similar conclusions may be drawn even when clouds are present. Figure 10 shows results of calculations for Sc II clouds of optical thickness varying from 0 to 40 over vegetated land and values of precipitable water of 1.6 and 3.1 cm. The spacing between equivalent lines in Figs. 9 and 10 is the same, suggesting that the effect of precipitable water can be taken into account uniquely without differentiating between clear and cloudy skies.

### *b. Cloud type*

The effect of cloud type on the relationship is illustrated in Fig. 11, which gives the results for the St II, Cu, and Ci cloud models, with optical thicknesses varying from 0 to 40 over an ocean surface. The results for the Sc-II model have been omitted for the sake of clarity, but, in fact, lie between the St-II and Cu lines and close to the Cu lines. Except for thick St clouds

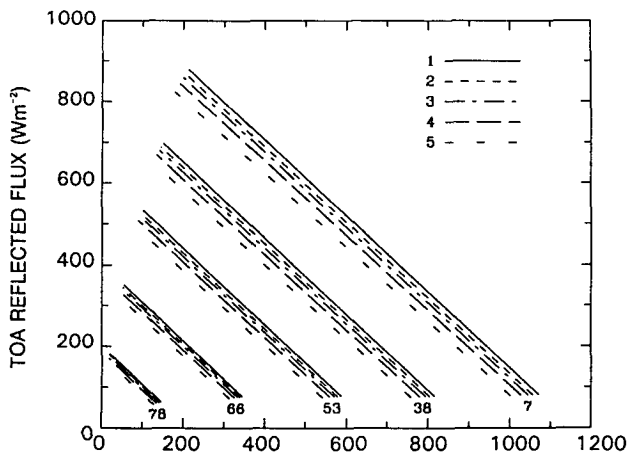


FIG. 9. Relationship between the flux absorbed at the surface and the flux reflected at the TOA for different precipitable water contents: 1.1, 1.6, 2.1, 3.1, and 5.1 cm designated by lines 1, 2, 3, 4, and 5, respectively, and a haze-optical thickness of 0.05. The lines are generated by joining points for clear skies over ocean and different snow/ice surfaces.

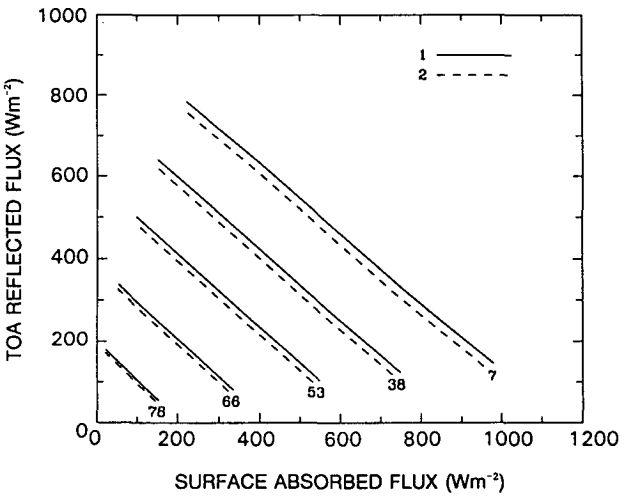


FIG. 10. Same as Fig. 9 but for Sc II with cloud-optical thickness ranging from 0 to 40 over vegetated land with two precipitable water contents: 1.6 cm (solid line) and 3.1 cm (dash line).

and Ci at SZAs larger than 72°, the relationship between reflected flux and surface-absorbed flux is linear for each of the cloud types considered. Furthermore, the relationship is only moderately sensitive to cloud type, the largest variations occurring between thick clouds at small SZAs and between water clouds and Ci at large SZAs. The effect of cloud type on the relationship is mainly on the slope parameter $\beta$, the intercept parameter $\alpha$ essentially not changing.

Because the cloud-droplet models for different cloud types have different extinction coefficients, different clouds types with the same optical thickness have different cloud-top heights that will affect the absorption by water vapor. To separate out the affect of changes in the amount of water vapor above the cloud from the affect of changes in the shape of the drop-size distribution, calculations for stratus clouds were repeated with an extinction coefficient identical to that for the stratocumulus cloud model. With the original extinction coefficient the stratus cloud-top height for $\tau = 40$ is 3.4 km, whereas with the modified extinction coefficient the cloud-top height is 1.3 km, the same as that for the stratocumulus cloud. For an SZA of 7°, the slope parameter, $\beta$, for the Sc-II model is 1.18, for the original St-II model $\beta = 1.12$, and for the St-II model, but with the modified extinction coefficient, $\beta = 1.14$. Lowering the cloud-top height by about 2 km does alter the slope parameter, but the change is significantly smaller than the changes in the slope parameter due to the changes in the optical properties of the two different drop-size distributions. The influence of cloud-top height was even less significant at larger SZAs.

### c. *Surface type*

Figure 12 shows the relationship for Sc-II cloud of varying optical thickness over ocean, vegetated land, desert, and snow with two grain sizes. The lines representing the results for different surface types are essentially indistinguishable except for ice at SZAs less than about 53°, and even then, the uncertainty due to absence of information about surface type is less than 20 W m$^{-2}$.

The relationships between reflected flux and flux absorbed at the surface, expressed as a function of cloud-optical thickness for clouds over ocean and as a function of surface type for clear skies with the surface changing from ocean to snow/ice of different grain

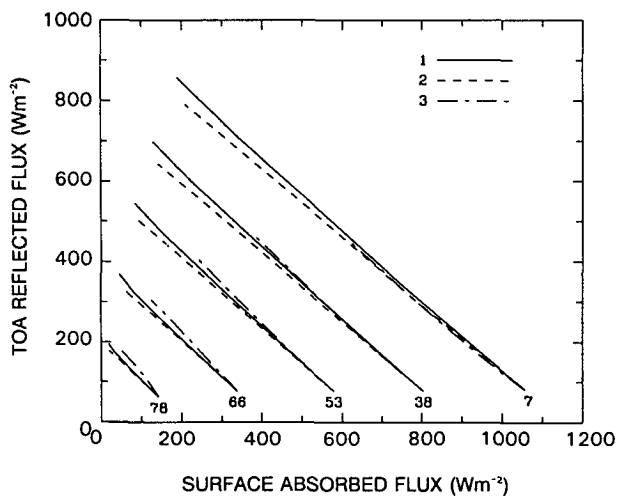


FIG. 11. Same as Fig. 9 but for different cloud types over ocean. Lines 1, 2, and 3 correspond to St II, Cu, and Ci, respectively. Cloud-optical thickness ranges from 0 to 40 for water clouds and from 0 to 10 for cirrus cloud. Precipitable water content is 1.6 cm, and haze optical thickness is 0.05.

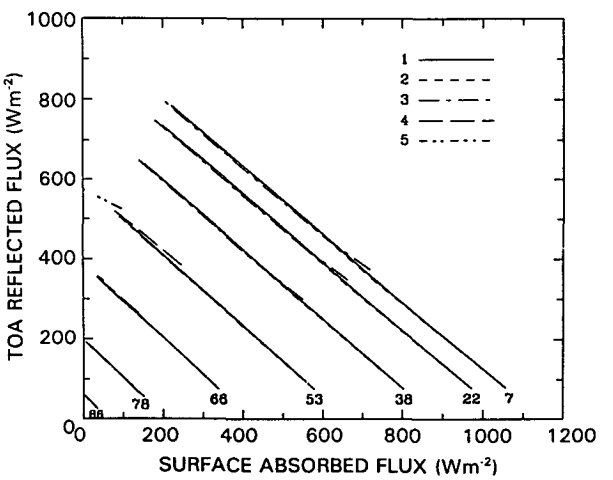


FIG. 12. Same as Fig. 9 but for Sc II over different surface types: ocean, vegetated land, desert, melting snow, and new snow, corresponding to curves 1 to 5, respectively. Precipitable water content is 1.6 cm, and haze optical thickness is 0.05.

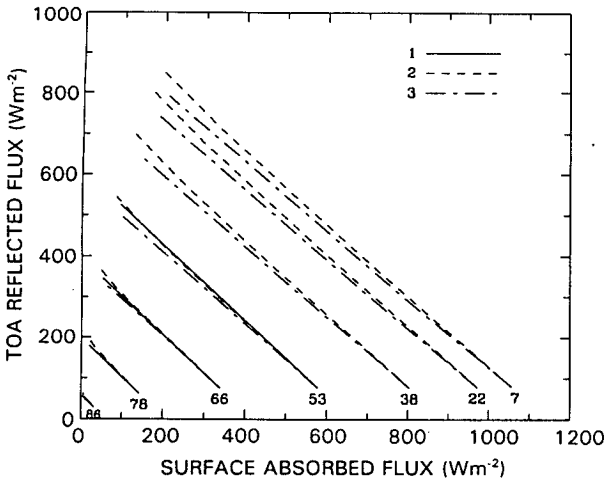


FIG. 13. Same as Fig. 9 but for clear skies, with the surface types changing from ocean to the various ages of snow (curve 1) and water clouds over ocean, St II (curve 2), Cu (curve 3) with optical thickness ranging from 0 to 40. Precipitable water content is 1.6 cm, and haze optical thickness is 0.05.

sizes, are compared in Fig. 13. The results are remarkably consistent, the results for clear skies lying between the results for the two different water cloud types for most SZAs. This implies that it may not be necessary to distinguish between clear and cloudy skies or different surface types in order to retrieve the surface-absorbed flux. This is of particular significance for the high latitudes where distinguishing between clear and cloudy skies from satellite data can be difficult (Li and Leighton 1991).

### *d. Aerosol*

The haze model 3 defined by Blanchet and List (1983) is used here to determine the effects of aerosol on the TOA–surface flux relationship since it represents the natural aerosol that is often observed in the summer Arctic. During summer, aerosol optical thickness ranges from about 0.03 to 0.1 (Shaw 1982). Therefore, three optical thicknesses of 0.0, 0.05, and 0.1 are included in simulations for clear-sky conditions, as shown in Fig. 14. The displacement of the curves from a clear atmosphere to a very hazy atmosphere is close to the displacement resulting from a change in precipitable water from 1.1 cm to 1.6 cm.

## 5. Parameterization

From the results of the last section it is seen that it is precipitable water and cloud type that exert the greatest influence on the parameters that link the net surface and TOA fluxes. This suggests that the following procedure should provide a simple but satisfactory parameterization of the flux absorbed at the surface in terms of the reflected flux at the TOA. First, a linear regression is made between the simulated fluxes reflected at the TOA and the fluxes absorbed at the surface for a fixed SZA and fixed amount of precipitable water but for different cloud optical thicknesses or surface types. Repeating the simulations for different SZAs allows the slope and intercept parameters of the regression to be parameterized in terms of SZA. Comparisons of the slope and intercept parameters from further simulations with different values of precipitable water, as well as the values obtained from the parameterization in terms of SZA, lead to a further parameterization of the slope and intercept in terms of precipitable water. Different parameterizations are obtained depending on whether the data are grouped according to cloud type, cloud water phase, or undifferentiated.

Plotted in Fig. 15 are the slope parameters versus the cosine of the SZA for clear skies with surfaces of ocean and snow/ice of different grain sizes, as well as four different cloud types, all with precipitable water of 1.6 cm. The slope for cirrus clouds is smallest in magnitude and changes most rapidly with SZA. For the cosine of the SZA within the range from 0.2 to 0.6, the slopes for clear skies and an ocean–ice surface are within the range of those for liquid clouds. Except at very small values of the cosine of the SZA, the slope for the clear case is almost independent of SZA. The solid curves in Fig. 15 are fits to the slopes given by $-\beta_0$, where

$$\beta_0(\mu) = 1 + (A + B \ln\mu). \quad (5)$$

The coefficients $A$ and $B$ are given in Table 2 for each of the five cases shown in Fig. 15.

In addition to SZA, precipitable water content has a weak effect on slope. This weak dependence is ac-

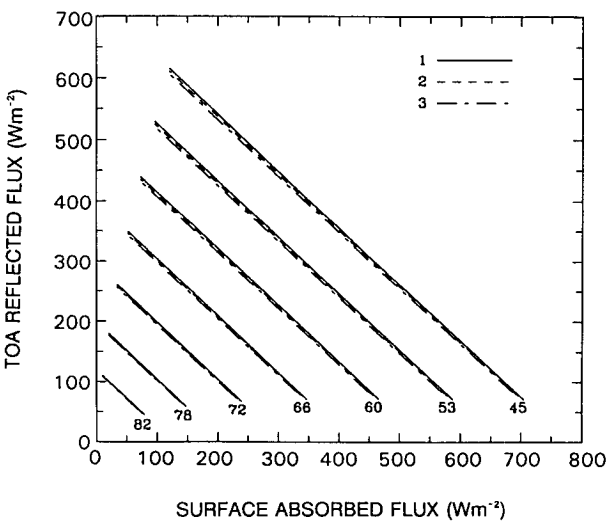


FIG. 14. Same as Fig. 9 but for clear skies, with the surface types changing from ocean to the various ages of snow for different optical thickness of haze: 0.0, 0.05, and 0.1, represented by curves 1 to 3, respectively. Precipitable water content is 1.6 cm.

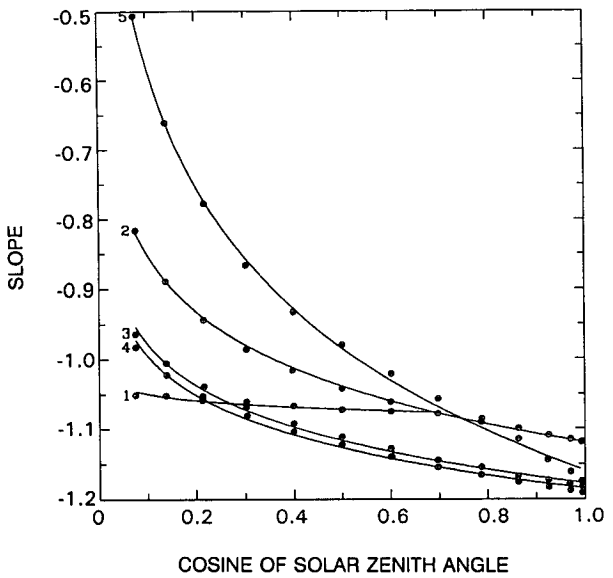


FIG. 15. Fits to the slope $-\beta_0(\mu)$ in the linear relationship between reflected flux at the TOA and absorbed flux at the surface. Curve 1 is for clear skies with the surface type changing from ocean to the various states of snow. Curves 2–5 represent cloudy skies over ocean for clouds of varying optical thickness: St II (curve 2), Sc II (curve 3), Cu (curve 4), and Ci (curve 5). Precipitable water content is 1.6 cm and haze optical thickness is 0.05. The curves are generated by the parameterization model given by (5), with coefficients given in Table 2.

counted for by introducing a small correction term $\Delta\beta$ to $\beta_0$, such that $\beta$ is given by

$$\beta(\mu, p) = \beta_0(\mu) + \Delta\beta(p) \tag{6}$$

with

$$\Delta\beta(p) = -0.0273 + 0.0216\sqrt{p}, \tag{7}$$

where $p$ denotes precipitable water content in centimeters. Although (7) is obtained from the clear-sky results shown in Fig. 9, it is found to be equally applicable to cloudy cases. Equations (6) and (7) imply that precipitable water tends to slightly increase the magnitude of $\beta$, as is also seen in Fig. 9.

In addition to the five individual cases included in Fig. 15, Table 2 also includes the values of the coefficients for fits to the mean slopes of the lines for St II and Cu clouds. These two cases exhibit the smallest and largest slopes, respectively, except for cirrus cloud, and so the parameterization based on these parameters is useful when no attempt is made to distinguish between water cloud types or between clear and cloudy skies.

TABLE 2. Coefficients of parameterization models to estimate surface-absorbed flux from TOA reflected flux.

| | Coefficients | | | |
|---|---|---|---|---|
| Model | *A* | *B* | *C* | *D* |
| Clear | 0.0815 | 0.0139 | −0.01124 | 0.1487 |
| St II | 0.1356 | 0.1045 | −0.00620 | 0.1415 |
| Sc II | 0.1766 | 0.0863 | −0.00769 | 0.1399 |
| Cu | 0.1838 | 0.0820 | −0.00801 | 0.1397 |
| Ci | 0.1591 | 0.2516 | 0.00255 | 0.1334 |
| Mean | 0.1609 | 0.0958 | −0.00696 | 0.1404 |

Similarly, the intercept parameter, expressed as a fraction of the incident flux at the TOA, is also fitted as a function of SZA and precipitable water by

$$\alpha(\mu, p) = \alpha_0(\mu) + \Delta\alpha(\mu, p), \tag{8}$$

where

$$\alpha_0(\mu) = 1 - \left[\left(\frac{C}{\mu} + \frac{D}{\sqrt{\mu}}\right)\right] \tag{9}$$

and

$$\Delta\alpha(\mu, p) = \frac{1}{\mu}[1 - \exp(-\mu)](0.0699 - 0.0683\sqrt{p}), \tag{10}$$

where coefficients $C$ and $D$ corresponding to each case are also given in Table 2. The computed and fitted intercepts, expressed as fluxes, for the lines representing surfaces of ocean and different types of snow/ice under clear skies and various precipitable water amounts are compared in Fig. 16. Fits to intercepts for cloudy conditions are as good as for the clear case.

As shown in Figs. 15 and 16, fits to the slope and

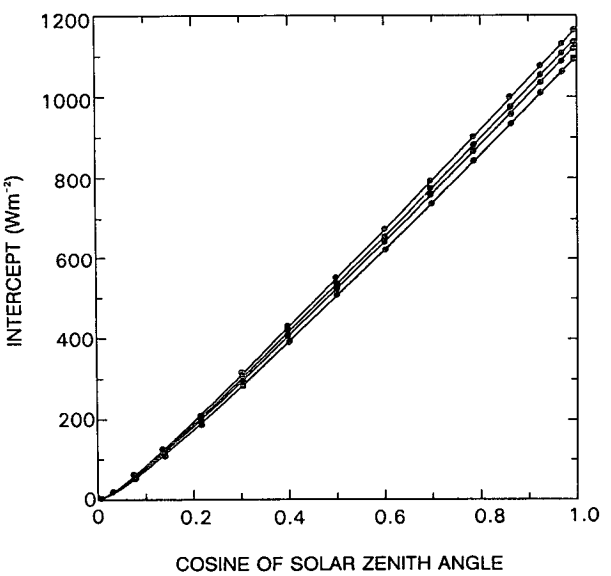


FIG. 16. Fits to the intercept in the linear relationship between reflected flux at the TOA and absorbed flux at the surface for clear skies with surface types changing from ocean to snow of different ages. The lines from top to bottom are for precipitable water contents: 1.1, 2.1, 3.1, and 5.1 cm. Haze optical thickness is 0.05. The curves are generated by the parameterization model with coefficients presented in Table 2.

intercept parameters are very good. In fact, errors in the estimates of surface-absorbed fluxes, resulting from inaccuracies in the fits, are generally less than 1 W $m^{-2}$.

## 6. Error analysis

To estimate the uncertainties that might be expected in determining the SRB from the reflected fluxes, radiative-transfer calculations are conducted for about 70 combinations of four cloud types with five-cloud optical thickness, seven surface categories, five water-vapor loadings, and three haze loadings. The results are plotted in Fig. 17, with pairs of solid and dashed lines bounding the data for a particular SZA. The distance between each pair of lines is a measure of the uncertainty in the estimation of surface-absorbed fluxes in the absence of any information other than SZA. The uncertainty can be very large, mainly due to the wide range of precipitable water and partly due to differences in cloud type.

Figure 18 shows the error histogram resulting from the application of the mean model whose parameters are given in the last line of Table 2, to the data of Fig. 17. Surface-absorbed fluxes estimated from the simulated TOA-reflected fluxes, with knowledge of SZA and precipitable water content, are compared with the fluxes calculated from the radiative-transfer model to determine the errors. The figure shows that by using a single model with known precipitable water, the uncertainty in the estimation of the surface-absorbed flux

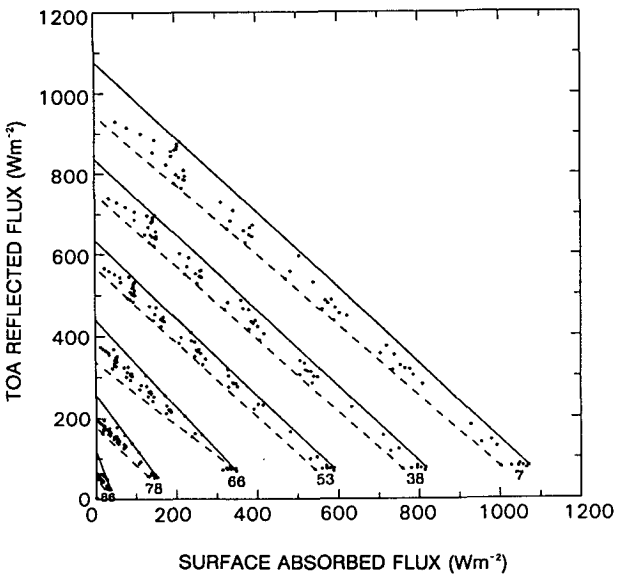


FIG. 17. Scattergram of reflected flux at the TOA versus absorbed flux at the surface from radiative transfer model calculations for about 70 combinations of four cloud types, five optical thickness, seven surface categories, five water vapor loadings, and three haze loadings. Solid and dashed lines are upper and lower bounds corresponding to a fixed SZA.

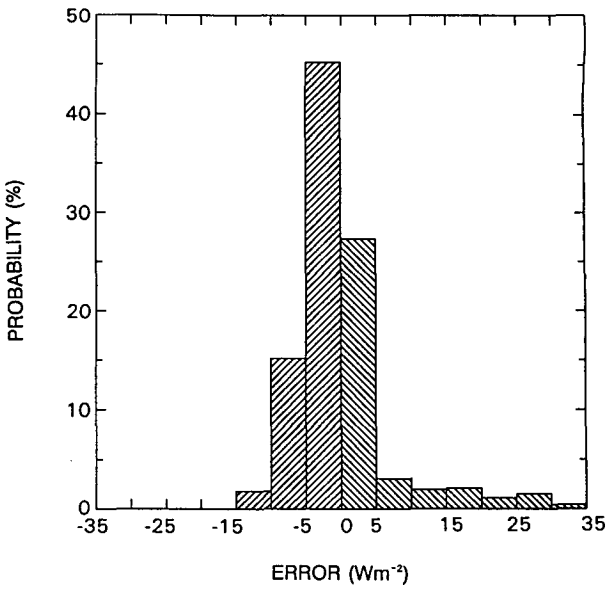


FIG. 18. Histogram of the error in the flux absorbed at the surface, resulting from the use of a single, mean parameterized model with the data of Fig. 17.

from the TOA-reflected flux is diminished substantially. More than 90% of the simulated surface-absorbed fluxes are reproduced to within 10 W $m^{-2}$ by the single model. Errors larger than 20 W $m^{-2}$ correspond to cases of cirrus clouds and arise because the linear relationships for cirrus cloud differ significantly from those for clear skies and skies covered by water clouds at large SZAs. If cirrus clouds are distinguished from water clouds and separate models are applied to each of these two cloud classes, no error larger than 20 W $m^{-2}$ is found. Such discrimination is possible from satellite measurements on the basis of differences in spectral emissivity, temperature, reflectance, and morphology (e.g., Arking and Childs 1985; Inoue 1987; Garand 1988). Recent theoretical studies by Masuda and Takashima (1990) show that changing the wavelengths of channel 3 in the AVHRR to around 1.6 $\mu$m will further enhance the ability of the AVHRR to distinguish the thermodynamic phase of cloud particles.

### *a. Uncertainty due to clouds*

To gain further insight into the uncertainty in the flux absorbed at the surface resulting from lack of knowledge of the water cloud type and optical thickness, the differences between the surface-absorbed fluxes obtained from the parameterization and the results from the transfer calculations for the cloud type that produced the largest discrepancy are calculated. The results are plotted as functions of SZA and normalized albedo (Fig. 19) for clouds over ocean and a fixed precipitable water of 1.6 cm. The normalized albedo $r_n$ is defined by

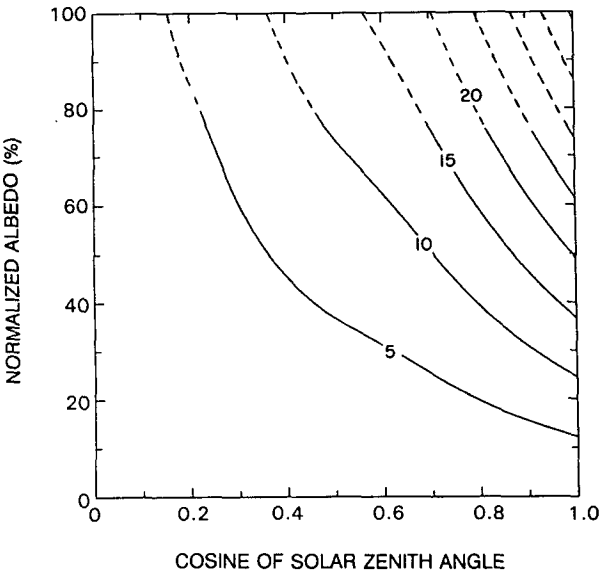


FIG. 19. Contour map of the error resulting from the application of the model that does not discriminate water cloud type, in the domain of SZA and normalized planetary albedo. The broken curves are based on extrapolated data. Normalized albedo ranges from 0 to 100% as cloud-optical thickness changes from zero to infinity.

$$r_n = \frac{r - r_{\min}}{r_{\max} - r_{\min}}, \tag{11}$$

where $r$ is the actual albedo, $r_{\min}$ is albedo for clear skies, and $r_{\max}$ is the albedo for infinite optical thickness obtained by extrapolating the parameterization to zero flux absorbed at the surface. The broken lines in Fig. 19 represent clouds with an optical thicknesses greater than 40, obtained by extrapolating the parameterization and the linear relationship between the TOA and surface fluxes. Support for the extrapolation is given by Schmetz (1989), who found a linear relationship between surface and TOA fluxes for optical thicknesses up to 725.

The uncertainty in the surface flux arising from the use of a single parameterization (the mean model) ranges from 0 to 35 W m$^{-2}$ as the cloud optical thickness increases from 0 to infinity and the cosine of the SZA increases from 0 to 1. The large uncertainties are, however, only found in a small area in the upper-right corner (small SZAs and thick cloud). The domain mean error is 7.3 W m$^{-2}$, and in about half the domain the error is less than 5 W m$^{-2}$. In the Arctic, the error is less than 10 W m$^{-2}$, as the SZA is always larger than 45°, and cloud optical thickness is usually less than 30 (Herman and Curry 1984). For SZAs larger than 53°, the uncertainty resulting from the use of the parameterization for clear skies with any type of surface is within the error estimate shown in Fig. 19, since the clear-sky lines in Fig. 13 lie within the range of the water cloud lines. This has the important implication that failure to identify clouds over snow/ice surfaces does not lead to an increase in the uncertainty in the estimation of the surface-absorbed flux.

### b. *Uncertainty due to precipitable water*

In the above error analysis, precipitable water is assumed to be known without any uncertainty. This is, of course, not realistic. If information about precipitable water is not available from radiosonde observations, numerical prediction models, or satellite measurements, climatological data may be employed. For example, if monthly mean values of precipitable water are used to derive daily mean surface-absorbed fluxes, the quantity that is needed to evaluate the random error in the estimate of the SRB is the standard deviation of the daily mean precipitable water $\delta p$. By differentiating (10) with respect to $p$ and multiplying by $F_0\mu$, where $F_0$ is the incident solar irradiance, the uncertainty in the estimation of surface-absorbed flux can be written as

$$\delta F = 0.034 F_0[1 - \exp(-\mu)] \frac{\delta p}{\sqrt{p}}. \tag{12}$$

Climatological values of $\delta p$ and $p$ are available from Oort and Rasmusson (1971) and Oort (1983). For the sake of simplicity, monthly zonal mean values of $\delta p$ and $p$ are employed here. The meridional variation of $p$, $\delta p$, and their combinations, $\delta p/p$ and $\delta p/\sqrt{p}$, are shown in Fig. 20 for three months. To examine the sensitivity of the surface flux to uncertainty in precipitable water, some investigators used a fixed relative error $\delta p/p$ (Cess and Vulis 1989; Schmetz 1989); others used a fixed absolute uncertainty $\delta p$ (e.g., Buriez et al. 1986). The results based on either of these approaches are only meaningful locally, since both $\delta p$ and $\delta p/p$ change significantly with latitude and season, as seen in Figs. 20b,c. Coincidentally, however, the ratio $\delta p/\sqrt{p}$ is found to be much more stable than both $\delta p$ and $\delta p/p$, especially at latitudes north of 40°N (Fig. 20d). This finding makes the analysis of the effect of precipitable water by (12) simple and more general. Based on the data in Fig. 20d, four values of the ratio $\delta p/\sqrt{p}$, 0.5, 0.6, 0.7, and 0.8 cm$^{-1/2}$, are employed to compute $\delta F$ (Fig. 21). The uncertainty resulting from the use of climatological values of precipitable water is strongly dependent on SZA. In the Arctic, for instance, where the ratio $\delta p/\sqrt{p}$ is close to 0.7 and the cosine of SZA is less than 0.7, the error is less than 15 W m$^{-2}$.

## 6. Conclusions

For many climate studies, the shortwave flux at the surface is an important quantity that is traditionally provided by ground-based measurements. These data, however, cannot satisfy the needs of global climate studies, owing to their limited and inhomogeneous coverage. Many attempts have been made to estimate

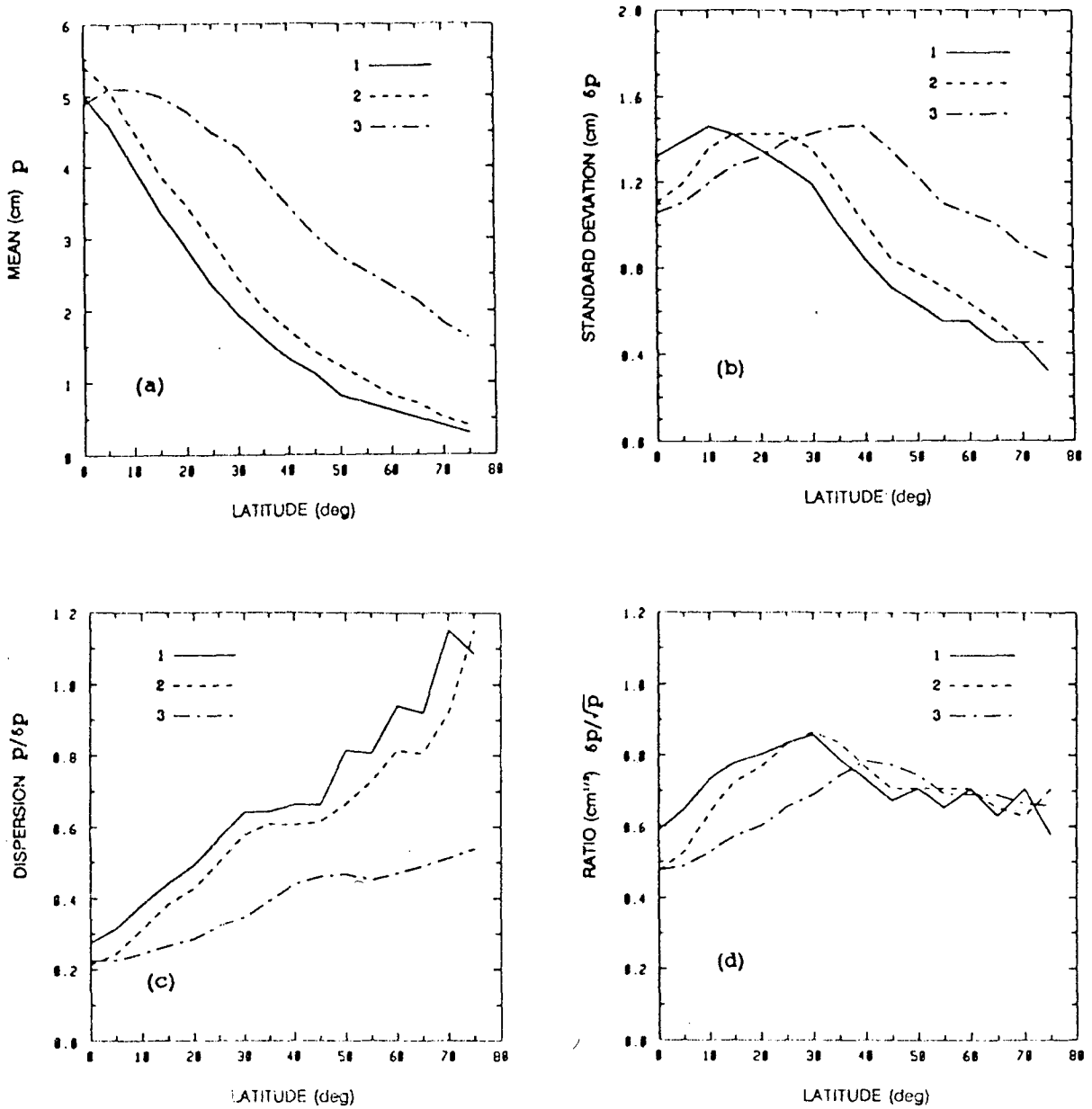


FIG. 20. Meridional variations of (a) $p$, the monthly mean precipitable water; (b) $\delta p$, standard deviation of the daily mean value of $p$; (c) $\delta p/p$; (d) $\delta p/\sqrt{p}$, for January, April, and July, represented by curves 1, 2, and 3, respectively.

surface radiative flux from satellite measurements. The majority of the methods are devoted to deriving downward insolation, while the more relevent quantity for climate studies is the net solar flux. This necessitates the determination of surface albedo, which is an even more difficult task.

Some previous studies have been reported in which the surface-absorbed solar flux is retrieved directly. This method is based on a linear relationship between column-absorbed and surface-absorbed fluxes. In this relationship, SZA is treated as an implicit parameter that links the net fluxes at the TOA and surface. The linear relationship turns out to be sensitive to many factors such as cloud optical thickness, surface type, etc. Since these parameters are not easily retrieved from satellite observations, the use of such a relationship is highly restricted.

Since it is the SZA that is the most important factor that relates the TOA and surface fluxes, and this is a quantity that can be easily and accurately determined, a better approach is to treat it as an explicit parameter while leaving other less easily derived quantities as implicit variables. Allowing either cloud optical thickness or surface albedo to vary leads to a new linear rela-

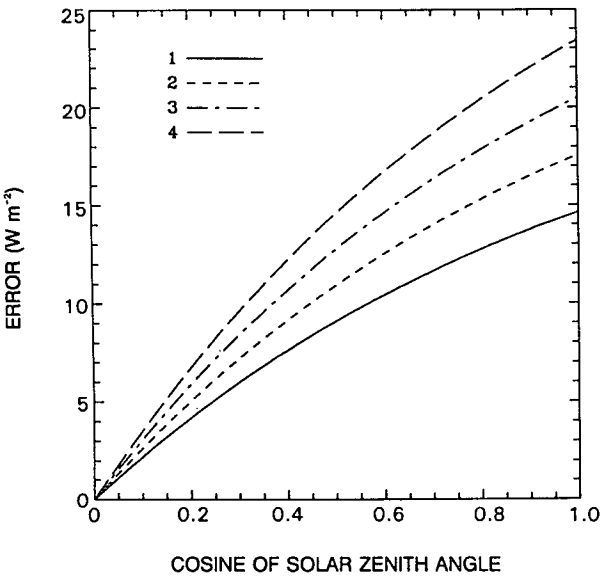


FIG. 21. Estimate of the error in the flux absorbed at the surface as a function of the cosine of SZA resulting from using the parameterized model with the climatological monthly mean precipitable water content for $\delta p/\sqrt{p}$ equal to (1) 0.5, (2) 0.6, (3) 0.7, and (4) 0.8.

tionship between the TOA and surface fluxes. As implicit factors, it is unnecessary to know their values in order to determine the surface-absorbed flux. More importantly, the relationship that results from varying the optical thickness of cloud and varying the surface albedo for clear skies is quite similar, which eliminates the necessity of distinguishing between clear and cloudy scenes.

Sensitivity studies reveal that apart from the SZA, the offset and slope of the linear relationship are mainly influenced by precipitable water and cloud type, respectively. Parameterized models are, therefore, developed in terms of these parameters and are applied to a simulated dataset. Error analysis suggests that cirrus cloud should be discriminated from water clouds, and precipitable water determined as precisely as possible in order to attain high accuracy in the estimation of surface-absorbed flux. It is found that the use of a single model for water clouds leads to 90% of the surface-absorbed fluxes being estimated to within 10 W $m^{-2}$, provided the precipitable water content is known. Use of climatological values of precipitable water may introduce an uncertainty of about 10 W $m^{-2}$ in instantaneous estimates of the flux absorbed at the surface but with smaller values for long-term averages. It must, however, be recognized that the range of conditions included in the present simulations is out of necessity limited, and undoubtedly, larger errors can occur. Furthermore, only errors resulting directly from the parameterization have been discussed, and errors related to the measurement of the TOA fluxes have been deliberately ignored. In practice, significant errors may result from the conversion of radiances to irradiances as a result of uncertainties in the angular-distribution models. In addition, if only narrowband radiances are available, further errors will be introduced from the narrowband to broadband conversion (Li and Leighton 1992). To assess the overall accuracy of the parameterization, a comprehensive comparison between results from the parameterization and surface-based observations, such as that carried out by Cess et al. (1991), but without restrictions on cloud and surface conditions, is required. It does, nevertheless, appear from the results of this theoretical study that the accuracy of 10 W $m^{-2}$ for the monthly mean solar flux absorbed at the surface and averaged over an area 250 × 250 $km^2$ required by climate studies (Suttles and Ohring 1986) can be attained.

*Acknowledgments.* We are grateful to Drs. S. C. Tsay and J. P. Blanchet for providing us their datasets. Software for automatic selection of mathematical models was kindly provided by Mr. J. Wang. The assistance of Ursula Seidenfuss with the diagrams is very much appreciated. This work was supported partially by grants from the Canadian Atmospheric Environment Service and the Natural Science and Engineering Research Council.

## REFERENCES

Arking, A., and J. D. Childs, 1985: Retrieval of cloud cover parameters from multispectral satellite images. *J. Climate Appl. Meteor.*, **24**, 322–333.

Blanchet, J.-P., and R. List, 1983: Estimation of optical properties of Arctic haze using a numerical model. *Atmos. Ocean*, **21**, 444–465.

Buriez, J. C., B. Bonnel, and Y. Fouquart, 1986: Theoretical and experimental sensitivity study of the derivation of the solar irradiance at the earth's surface from satellite data. *Beitr. Phys. Atmos.*, **59**, 263–281.

Cess, R. D., and I. L. Vulis, 1989: Inferring surface solar absorption from broadband satellite measurements. *J. Climate*, **2**, 974–985.

——, E. G. Dutton, J. J. DeLuisi, and F. Jiang, 1991: Determining surface solar absorption from broadband satellite measurements for clear skies: Comparison with surface measurements. *J. Climate*, **4**, 236–247.

Davies, R., 1980: Fast azimuthally dependent model of the reflection of solar radiation by plane-parallel clouds. *Appl. Opt.*, **19**, 250–255.

——, W. L. Ridgway, and K. E. Kim, 1984: Spectral absorption of solar radiation in cloudy atmospheres: A 20 $cm^{-1}$ model. *J. Atmos. Sci.*, **4**, 2126–2137.

Dedieu, G., P. Y. Deschamps, and Y. H. Kerr, 1987: Satellite estimation of solar irradiance at the surface of the earth and of surface albedo using a physical model applied to Meteosat data. *J. Climate Appl. Meteor.*, **26**, 79–87.

Fritz, S., P. Rao, and M. Weinstein, 1964: Satellite measurements of reflected solar energy and the energy received at the ground. *J. Atmos. Sci.*, **21**, 141–151.

Garand, L., 1988: Automated recognition of oceanic cloud patterns. Part I: Methodology and application to cloud climatology. *J. Climate*, **1**, 20–39.

Gautier, C., G. Diak, and S. Masse, 1980: A simple physical model to estimate incident solar radiation at the surface from GOES satellite data. *J. Appl. Meteor.*, **19,** 1005–1012.

Herman, G. F., and J. A. Curry, 1984: Observational and theoretical studies of solar radiation in Arctic stratus clouds. *J. Climate Appl. Meteor.*, **23,** 5–24.

Inoue, T., 1987: A cloud type classification with NOAA 7 split-window measurements. *J. Geophys. Res.*, **92,** 3991–4000.

Iqbal, M., 1983: *An Introduction to Solar Radiation.* Academic Press, 390 pp.

Klink, J. C., and K. J. Dollhopf, 1986: An evaluation of satellite-based insolation estimates for Ohio. *J. Climate Appl. Meteor.*, **25,** 1741–1751.

Kneizys, F. X., E. P. Shettle, W. O. Gallery, J. H. Chetwynd, Jr., L. W. Abreu, J. E. A. Selby, S. A. Clough, and R. W. Fenn, 1983: Atmospheric transmittance/radiance: Computer code LOWTRAN 6, AFGL-TR-83-0187, 200 pp.

Li, Z., and H. G. Leighton, 1991: Scene identification and its effect on cloud radiative forcing in the arctic. *J. Geophys. Res.*, **96,** 9175–9188.

——, and ——, 1992: Narrowband to broadband conversion with spatially autocorrelated reflectance measurements. *J. Appl. Meteor.*, **31,** 421–432.

Masuda, K., and T. Takashima, 1988: Sensitivity of radiation absorbed in the ocean to atmospheric and oceanic parameters in the short wavelength region. Part 1: Cloudless atmosphere. *J. Meteor. Soc. Japan,* **66,** 617–628.

——, and ——, 1990: Deriving cirrus information using the visible and near-IR channels of the future NOAA-AVHRR radiometer. *Remote Sens. Environ.*, **31,** 65–81.

McClatchey, R. A., R. W. Fenn, J. E. A. Selby, F. E. Volz, and J. S. Garing, 1971: Optical properties of the atmosphere. Air Force Cambridge Rep. AFCRL-71-0279, 85 pp. [Available from Air Force Cambridge Research Laboratory, Cambridge, MA.]

Möser, W., and E. Raschke, 1983: Mapping of global radiation and of cloudiness from METEOSAT image data. *Meteor. Rundsch.*, **36,** 33–41.

Oort, A. H., 1983: Global atmospheric circulation statistics, NOAA Professional Paper No. 14, 180 pp. [Available from U.S. Government Printing Office, Washington, D.C.]

——, and E. M. Rasmusson, 1971: *Atmospheric Circulation Statistics.* NOAA Professional Paper No. 5, U.S. Govt. Printing Office, Washington, D.C., 323 pp.

Pinker, R. T., and J. A. Ewing, 1985: Modeling surface solar radiation: Model formulation and validation. *J. Climate Appl. Meteor.*, **24,** 389–401.

Ramanathan, V., 1986: Scientific use of surface radiation budget data for climate studies. Report of the Workshop on Surface Radiation Budget for Climate Applications.

Rawlins, F., 1989: Aircraft measurements of the solar absorption by broken cloud fields: A case study. *Quart. J. Roy. Meteor. Soc.*, **115,** 365–382.

Schmetz, J., 1984: On the parameterization of the radiative properties of broken clouds. *Tellus,* **36A,** 417–432.

——, 1989: Towards a surface radiation climatology: Retrieval of downward irradiances from satellites. *Atmos. Res.*, **23,** 287–321.

Shaw, G., 1982: Atmospheric turbidity in the polar regions. *J. Appl. Meteor.*, **21,** 1080–1088.

Stephens, G. L., 1978: Radiation profiles in extended water clouds II: Parameterization schemes. *J. Atmos. Sci.*, **35,** 2111–2122.

——, 1979: Tech. Paper No. 36: Optical properties of eight water cloud types. 35 pp. [Available from CSIRO Division of Atmospheric Physics.]

Suttles, J. T., and G. Ohring, 1986: Report of the workshop on surface radiation budget for climate applications, WCP-115, World Meteorological Organization, 144 pp.

Tarpley, J. D., 1979: Estimating incident solar radiation at the surface from geostationary satellite data. *J. Appl. Meteor.*, **18,** 1172–1181.

Tsay, S. C., K. Stamnes, and K. Jayaweera, 1989: Radiative energy budget in the cloudy and hazy Arctic. *J. Atmos. Sci.*, **46,** 1002–1018.

Warren, S. G., and W. J. Wiscombe, 1980: A model for the spectral albedo of snow. Part II: Snow containing atmospheric aerosols. *J. Atmos. Sci.*, **37,** 2734–2745.

Wiscombe, W. J., and S. G. Warren, 1980: A model for the spectral albedo of snow. Part I: Pure snow. *J. Atmos. Sci.*, **37,** 2712–2733.